Materials Science-Poland, Vol. 23, No. 1, 2005

Formation of nanostructured Tb^{3+}-doped yttrium aluminium garnets by the glycol route

PIOTR MAZUR[1*], DARIUSZ HRENIAK[1],
JANNE NIITTYKOSKI[2], WIESŁAW STRĘK[1], JORMA HÖLSÄ[2]

[1]Institute of Low Temperature and Structure Research, Polish Academy of Sciences,
P.O. Box 1410, 50-950 Wrocław, Poland

[2]Department of Chemistry, University of Turku, FI-20014 Turku, Finland

Terbium-doped nanocrystalline yttrium aluminium garnet phases, $Y_3Al_5O_{12}:Tb^{3+}$ ($YAG:Tb^{3+}$), were obtained by using rare-earth nitrates as the starting materials, together with citric acid and ethylene glycol according to the Pechini method. Thermogravimetric and differential thermal analysis were used to study the thermal decomposition of the precursor gels and the formation of nanocrystalline $YAG:Tb^{3+}$. An increase in garnet nanocrystallite size from 20 to 40 nm with annealing temperature increasing from 800 to 1160 °C was evidenced with X-ray powder diffraction measurements. The intensity as well as the decay times of both $^5D_3$ and $^5D_4$ emissions of $Y_3Al_5O_{12}:Tb^{3+}$ were not found to depend on annealing and were thus independent of crystal size.

Key words: *garnet; YAG, nanocrystals; luminescence; terbium*

1. Introduction

It is well known that polycrystalline yttrium aluminium garnets, $Y_3Al_5O_{12}$ (YAG), doped with selected rare earth ions (Tb^{3+}, Eu^{3+}, Ce^{3+}) can be used as efficient phosphors [1–3]. However, the standard synthesis of these materials as single crystals requires temperatures above 1600 °C and intricate conditions during the crystal growth process. Due to these reasons, garnets have been developed for optical applications in other forms, such as micrometric phosphor powders, scintillator ceramics, thin films, and laser ceramics [4–7]. In recent years, a growing number of investigations have been focused on the production of nanocrystalline YAG powders, which have optical properties comparable to YAG powders of micrometer size. For example, the first attempts to construct a solid-state laser based on polycrystalline ceramics were re-

*Corresponding author, e-mail: mazur@int.pan.wroc.pl.

ported some time ago [5]. YAG powders doped with terbium and europium ions are potential candidates for materials in luminescent lamps and display applications [3].

Yttrium aluminium garnets are conventionally manufactured by a solid-state reaction between the rare earth oxides, Y_2O_3 and Al_2O_3 at high temperatures, typically around 1600 °C. In the last decade, several low temperature processes such as co-precipitation [8], the sol-gel method [9, 10], combustion [11–13], and hydrothermal synthesis [14] have been developed to fabricate garnets with fine particle size. The fabrication technology of high-quality nanocrystalline YAG powders, however, is still subject to intense studies since the optical properties of nanocrystals are strongly dependent on the size of individual nanocrystals and conditions of syntheses. Therefore, any information about the nature and formation of crystalline phases is of great importance.

In the present report, the results of studies concerning the formation and properties of Tb^{3+}-doped yttrium aluminium garnet nanocrystals are revealed. They were obtained by a glycol-route method, also called Pechini's method. Formation was investigated by the TG and DTA methods, which allow the weight loss of the sample to be characterized in detail and additionally gives information about the occurrence of energetic processes [15] during annealing, particularly the decomposition of yttrium nitrate [16] and carbonate [17]. Results of the thermal analysis of the formation of the nanocrystalline YAG:Tb^{3+} phase were compared with those obtained by luminescence methods and X-ray powder diffraction (XRD).

2. Experimental

The preparation method of nanocrystalline yttrium aluminium garnets has been reported elsewhere [18, 19]. Briefly, aqueous nitrate solutions of yttrium and terbium were prepared by dissolving high purity Y_2O_3 (99.999 %) and Tb_4O_7 (99.99 %) with ultrapure HNO_3. Yttrium nitrate and aluminium chloride (99.9995 %) were then dissolved in Stoichiometric amounts in a mixture of aqueous citric acid and ethylene glycol to give a molar ratio of 3:5:50:20. Terbium nitrate was added to the homogeneous solution to give a nominal concentration of terbium vs. yttrium of 2 mole %. The solutions obtained were ultrasonically stirred for two hours. Then they were heated at 80 °C for several hours and dried at 100 °C for seven days in order to obtain gels. Samples of the crushed gel were heat-treated at selected temperatures between 800 and 1160 °C in air in an electric furnace to obtain single phases of yttrium aluminium garnet.

Thermogravimetric curves were recorded in air (flow rate: 100 $cm^3 \cdot min^{-1}$) with a TA Instruments SDT 2960 Simultaneous DTA-TGA thermoanalyser. The sol-gel and solid-state reactions were studied in the temperature range from 25 °C to 1160 °C, with a heating rate of 5 $K \cdot min^{-1}$. α-Al_2O_3 was used as the DTA reference material. The structure and crystallinity of the samples were evaluated by X-ray powder diffraction with a Stoe powder diffractometer equipped with a position-sensitive detector. Filtered $CuK_{\alpha 1}$ radiation (λ = 1.5406 Å) and a 2θ step of 0.02 degrees was

used in the 2θ range 15–60 degrees. TEM micrographs were recorded with a JEM-3010 (JEOL) electron microscope.

The luminescence spectra of YAG:Tb^{3+} between 300 and 900 nm were measured at room temperature with an ISA Jobin-Yvon TRW 1000 monochromator equipped with standard detection as well as data acquisition and treatment systems. All spectra recorded were corrected for the sensitivity of the experimental set-up. The resolution of the spectra was not better than 0.2 nm. The 266 nm line of the 4th harmonic of an Nd:YAG laser was used as the excitation source. Emission lifetimes were measured with a Tektronics TDS 380 oscilloscope and the 308 nm line of a Lambda Physik LPX 100 excimer laser as the excitation source.

3. Results and discussion

3.1. DTA-TG analysis

The TG and DTA curves of dried gels (Fig. 1) show that the process of formation of $Y_3Al_5O_{12}$:Tb^{3+} involves an almost continuous weight loss up to 1000 °C, although most of the loss occurs at rather low temperatures, below 400 °C. The TG curves indicate an overall weight loss of approximately 95%. The weight loss observed in the

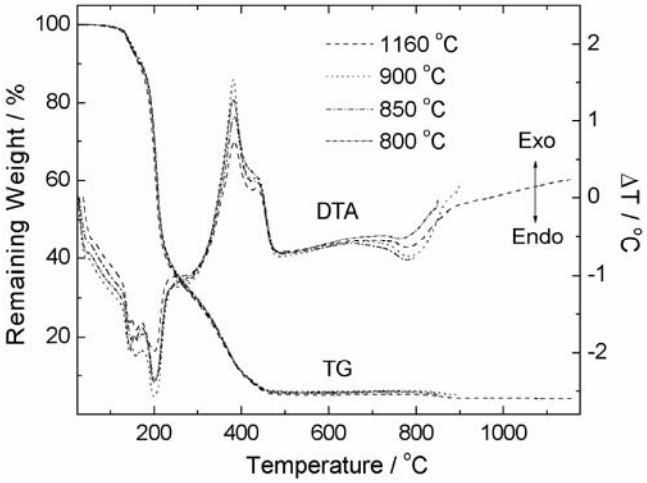

Fig. 1. Thermogravimetric (TG) and differential thermal analysis (DTA) curves of the glycol-route reactions in fabricating $Y_3Al_5O_{12}$:Tb^{3+} (sample weight: c.a. 10 mg, heating rate: 5 $K \cdot min^{-1}$, airflow rate: 100 $cm^3 \cdot min^{-1}$)

very first part of the TG curve (below 100 °C) is mainly due to the evaporation of organic solvents, since the endothermic signal in the DTA curve is rather weak. The stronger endothermic signal at 150 °C, accompanied by a rather moderate weight loss above 100 and below 180 °C, can be attributed to the removal of water [9], which can

be relatively strongly bound. The next, much stronger weight loss with an endothermic DTA signal in the temperature range of 150–200 °C is due to the removal of NO and NO_2 [12, 16], as a result of the decomposition of nitrates. This is in agreement with low thermal stability of the heavier rare earth (and yttrium) nitrates [20]. Even oxynitrates ($RONO_3$) decompose below 500 °C.

The decomposition of organic matter occurs practically simultaneously [2], which is oxidized immediately to CO and CO_2, causing two very strong exothermic peaks in the DTA curves at 380 and 435 °C. This decomposition is practically over just below 500 °C, though it is possible that some yttrium oxycarbonates may well resist decomposition at higher temperatures, up to 600 °C [21]. Taken into the vigorous decomposition of organic matter and evolution of CO, some carbon might be left in the samples and the total oxidation of organic matter may not be complete. The final, albeit rather weak weight loss observed in the range of 850–900 °C may well be due to the burning of the residual carbon. This reaction should be exothermic, but in the DTA curves a broad endothermic signal is first observed, possibly due to crystallization and the formation of the garnet phase [8, 15]. The exothermic signal of burning carbon may well be masked by this endothermic signal. A sharp DTA signal, however, has been found, typical of the transformation of precursors into a crystalline form of garnet [15]. On the other hand, crystallization is a physical process and should not be accompanied by any weight change. This supports the presence of some residual carbon, as does the observation that in reaction conditions with excess oxygen this weight loss is very small or even not observed, and consequently the DTA signal is weak, too [12]. The amount of residual carbon in the products heated at 800 °C has been determined to be as high as 3% [9], and this amount decreases considerably as a result of heating at temperatures higher than 800 °C.

3.2. X-Ray powder diffraction studies

The crystallinity as well as phase purity of $Y_3Al_5O_{12}:Tb^{3+}$ nanocrystalline samples were characterized by X-ray powder diffraction (XRD). All the diffraction reflections observed could be indexed with those assigned to cubic $Y_3Al_5O_{12}$ [JCPDS#33-40] (Fig. 2). Irrespective of the annealing temperature above 800 °C, the phase purity of the samples was found to be excellent. The width of the reflections, measured as FWHM values, were found to depend on the annealing temperature: the higher the temperature, the sharper were the reflections. This kind of evolution of the FWHM values was to be expected and was used to determine the crystallite size of nanoparticles. The average size of nanoparticles was determined from the broadening of diffraction reflections according to the Scherrer's formula [22]. To obtain true diffraction profiles for various reflections, corrections for instrumental broadening were applied using the FWHM values of Si as a standard. The average size of the nanocrystals was found to be dependent on the annealing temperature, and increased in the temperature range of 800–1160 °C from 20 to 40 nm, respectively. These results are

in good general agreement with TEM images (Fig. 3), which also show that the particles have rather uniform shapes and that the size distribution is not exceedingly large if the rather pronounced tendency to aggregate is omitted.

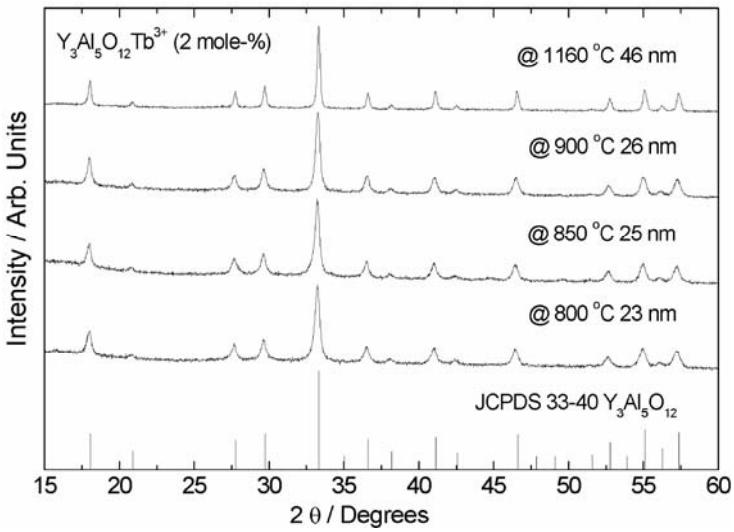

Fig. 2. XRD patterns of the $Y_3Al_5O_{12}:Tb^{3+}$ (2 mole %) powder samples ($CuK_{\alpha 1}$ radiation, λ = 1.5406 Å)

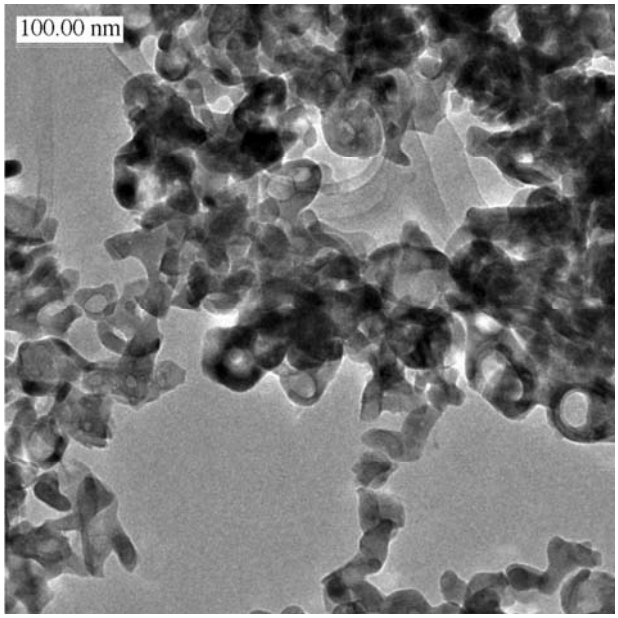

Fig. 3. TEM images of $Y_3Al_5O_{12}:Tb^{3+}$ (2 mole %) nanocrystals heated at 800 °C

3.3. Luminescence Spectra of YAG:Tb^{3+}

The emission spectra of YAG:Tb^{3+} nanocrystals were measured at room temperature as a function of the annealing temperature (Fig. 4). The spectra consist of characteristic peaks in the UV-blue and blue-green spectral regions, which correspond to the $^5D_3 \rightarrow {}^7F_J$ (J = 6–0) and $^5D_4 \rightarrow {}^7F_{J'}$ (J' = 6, 5, 4, 3) transitions, respectively. All the observed emission bands of YAG:Tb^{3+} nanopowders were found and resolved, even after annealing at 800 °C. This points out that already at this low temperature the samples seem to be well crystallized. It should be noted, however, that since the degeneracy of both emitting levels and terminal ones is rather high, the number of individual transitions between the crystal field levels of each $^{2S+1}L_J$ is high, too. Accordingly, the use of Tb^{3+} luminescence as a structural probe requires low measuring temperatures in contrast to the Eu^{3+} ion, the luminescence of which may be used even at room temperature to reliably examine the luminescence characteristics and impurities of samples.

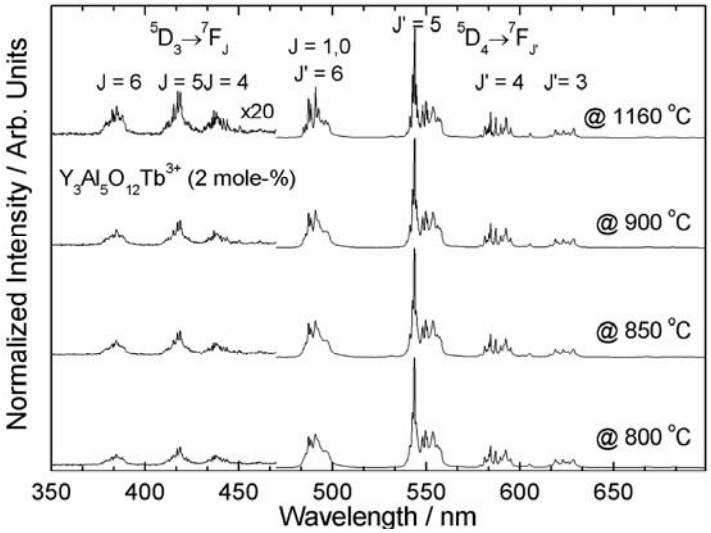

Fig. 4. Luminescence spectra of $Y_3Al_5O_{12}$:Tb^{3+} (2 mole %) powders derived in glycol-route process

The UV-blue emission of the Tb^{3+} ion ($^5D_3 \rightarrow {}^7F_J$) was observed to be much weaker compared to blue-green emission ($^5D_4 \rightarrow {}^7F_{J'}$) (Fig. 4). The weakness of the blue emission may be rationalized by the concentration quenching associated with the cross-relaxation process ($^5D_3 \rightarrow {}^5D_4$) $\leftrightarrow$ ($^7F_6 \rightarrow {}^7F_0$), which results in enhanced emission from the $^5D_4$ level at the expense of $^5D_3$ emission.

In order to analyse the influence of annealing on the luminescence dynamics and to observe the possible existence or appearance of non-radiative relaxation paths due to crystallite size, the luminescence decays of YAG:Tb^{3+} nanocrystallites were recorded at room temperature. Examples of luminescence decay curves, measured for

the blue $^5D_3 \rightarrow {}^7F_5$ (418.7 nm, excitation at 308 nm) and green $^5D_4 \rightarrow {}^7F_5$ (543.6 nm, excitation to the $^7F_6 \rightarrow {}^5D_4$ transition at 484 nm) transitions in YAG:Tb^{3+} nanocrystallites annealed at 800 °C, are shown in Fig. 5.

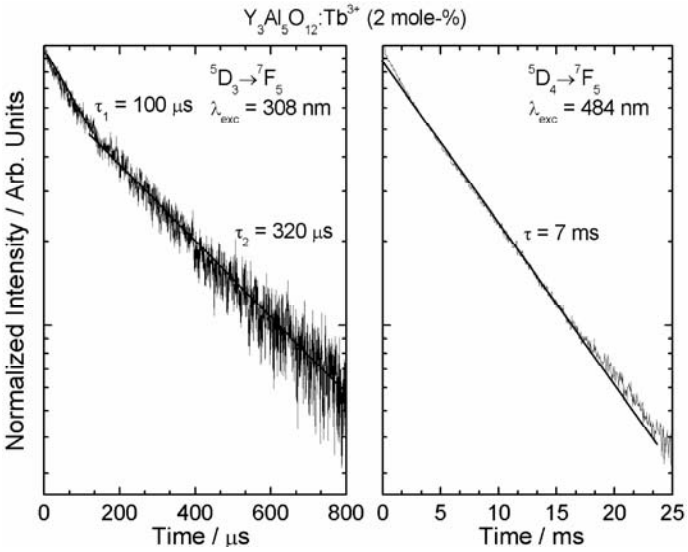

Fig. 5. Luminescence decay curves of the $^5D_3 \rightarrow {}^7F_5$ (left) and $^5D_4 \rightarrow {}^7F_5$ (right) transitions in $Y_3Al_5O_{12}$:Tb^{3+} (2 mole %) nanocrystallites

The decay curves for the blue $^5D_3$ emission are composed of two exponential components, a fast component with the decay time of 100 μs and a slower one with 320 μs. The multicomponent decay time of the $^5D_3$ emission is evidently due to the fact that excitation was not directly to the $^5D_3$ level, but to higher excited levels of the $4f_8$ electron configuration, or even to the next excited electron configuration, $4f_75d_1$. Different excitation paths result in different decay times for the $^5D_3$ emission. The decay curves for the green emission were almost perfectly exponential. The luminescence decay time of $^5D_4 \rightarrow {}^7F_5$ luminescence was determined to be c.a. 7 ms. The $^5D_3$ emission decays observed were much shorter than the $^5D_4$ ones as expected, since emission from the $^5D_3$ level must compete with other processes such as cross-relaxation and multi-phonon de-excitation to the $^5D_4$ level. No significant effect of the annealing temperature and thus crystal size was observed on the measured decay profiles.

4. Conclusions

The formation of $Y_3Al_5O_{12}$:Tb^{3+} nanocrystalline powders was analysed by thermogravimetric and differential thermal analyses. It was found that beyond drying, several different processes occurred before the proper formation of nanocrystalline YAG:Tb^{3+}, being associated with the decomposition of nitrates, (partial) oxidation

and decomposition of organic matter, decomposition of carbonates, and finally the burning of residual carbon. The formation of nanocrystalline YAG:Tb^{3+} was achieved already at 780 °C, although the removal of impurities such as carbon demanded a slightly higher annealing temperature. The nanocrystallites obtained demonstrated an increase in crystal size from 20 to 40 nm for annealing taking place at 800 and 1160 °C, respectively. No significant effect of the annealing temperature was observed in the static and dynamic properties of the $^5D_3$ and $^5D_4$ emissions. The glycol route thus offers a simple and inexpensive method for fabricating good quality YAG:Tb^{3+} nanocrystals with luminescence properties comparable to those of microsized crystals.

Acknowledgements

The authors thank M. Wolcyrz for the XRD measurements and E. Zawadzak for the TEM graphs. This work was partially supported by the KBN grant PBZ-KBN-095/T08/. J.N. and J.H. acknowledge the financial support from the Academy of Finland (Project No. 204547).

References

[1] SHINOYA S., YEN W.M., *Phosphor Handbook*, CRC Press, Boca Raton, 1998.
[2] ZHOU Y.H., LIN J., WANG S.B., ZHANG H.J., Opt. Mater., 20 (2002), 13.
[3] CHOE J.Y., RAVICHANDRAN D., BLOMQUIST S.M., KIRCHNER K.W., FORSYTHE E.W., MORTON D.C., J. Lumin., 93 (2001), 119.
[4] IKESUE A., FURUSATO I., KAMATA K., J. Amer. Ceram. Soc., 78 (1995), 225.
[5] IKESUE A., KINOSHITA T., KAMATA K., YOSHIDA K., J. Amer. Ceram. Soc., 78 (1995), 1033.
[6] LU J., UEDA K., YAGI H., YANAGITANI T., AKIYAMA Y., KAMINSKII A.A., J. Alloys Comp., 341 (2002), 220.
[7] GRESKOVICH C., CHERNOCH J.P., J. Appl. Phys., 44 (1973), 4599.
[8] WANG H., GAO L., NIIHARA K., Mater. Sci. Eng. A, 288 (2000), 1.
[9] PILLAI K.T., KAMAT R.V., VAIDYA V.N., SOOD D.D., Mater. Chem. Phys., 44 (1996), 255.
[10] VAQUEIRO P., LÓPEZ-QUINTELA M.A., J. Mater. Chem., 8 (1998), 161.
[11] SHIKAO S., JIYE W., J. Alloys Comp., 327 (2001), 82.
[12] ROY S., WANG L., SIGMUND W., ALDINGER F., Mater. Lett., 39 (1999), 138.
[13] MCKITTRICK J., SHEA L.E., BACALSKI C.F., BOSZE E.J., Displays, 19 (1999), 169.
[14] INOUE M., OTSU H., KOMINAMI H., INUI T., J. Alloys Comp., 226 (1995), 146.
[15] PARK C.-H.., PARK S.-J., YU B.-Y., BAE H.-S., KIM C.-H.., PYUN C.-H., GUANG-YAN H., J. Mater. Sci. Lett., 19 (2000), 335.
[16] UNFRIED P., Thermochim. Acta, 303 (1997), 119.
[17] MOSCARDINI D'ASSUNÇÃO L., IONASHIRO M., RASERA D.E., GIOLITO I., Thermochim. Acta, 219 (1993), 225.
[18] HRENIAK D., STRĘK W., MAZUR P., PAZIK R., ZĄBKOWSKA-WACŁAWEK M., Opt. Mater. 26 (2004), 117.
[19] HRENIAK D., STRĘK W., MAZUR P., Mater. Sci., 20 (2002), 39.
[20] WENDLANDT W.W., BEAR J.L., J. Inorg. Nucl. Chem., 12 (1960), 276.
[21] HÖLSÄ, J., TURKKI, T., Thermochim. Acta, 190 (1991), 335.
[22] KLUG P., ALEXANDER L.E., *X-Ray Diffraction Procedure*, Wiley, New York, 1954, Chapt. 9.

Received 20 April 2004
Revised 9 November 2004